Research Article Vol. 32, No. 14 / 1 Jul 2024 / Optics Express 25180
Optics EXPRESS

SBS suppression in fiber amplifiers with a broadband seed

JEFFREY O. WHITE,[1,*] DAVID M. BROWN,[2] ANDY GOERS,[2] BRICE M. CANNON,[3] AND CURTIS R. MENYUK[1]

[1] University of Maryland, Baltimore County, 5200 Westland Blvd., Baltimore, MD 21227, USA
[2] Johns Hopkins Applied Physics Laboratory, 11100 Johns Hopkins Rd., Laurel, MD 20723, USA
[3] Currently with MITRE Corporation, 7525 Colshire Dr., McLean, VA 22102, USA
[*] jeffrey.o.white@opticamember.org

Abstract: We present a scalar, time-dependent, plane-wave model for stimulated Brillouin scattering (SBS) within a fiber amplifier having a seed linewidth comparable to, or greater than, the Brillouin frequency shift. The broadband model introduces the existence of a backward anti-Stokes wave, in addition to the Stokes wave present in the narrowband model. The model also incorporates a Fresnel reflection within the fiber or at the exit face. In the absence of Fresnel reflections, the SBS threshold increases linearly with seed linewidth, up to linewidths of at least three times the Brillouin frequency shift. In the presence of Fresnel reflections that seed the Stokes wave, the threshold increases sub-linearly, which agrees with previously reported experimental results. For non-zero reflections and modulation formats with very compact spectra, the threshold can decrease with bandwidth in the region 16–24 GHz due to seeding of the Stokes wave.

1. Introduction

High-power fiber amplifiers with compact spectra are advantageous for both coherent combining [1] and spectral combining [2,3]. Current narrow-linewidth, high-power, nearly-fundamental-mode fiber amplifiers operate near the threshold for stimulated Brillouin scattering (SBS). Recent techniques for raising the threshold include developing fibers with low nonlinearity [4,5], engineering seed spectra [6–8], and synchronous amplitude and phase modulation of the seed [9]. Scaling the power to multiple kilowatts from a single aperture is accomplished by using a seed linewidth that is 10's of GHz, i.e., 100's of times larger than the ~100 MHz Brillouin linewidth. In this regime, models that incorporate the usual assumption that the laser linewidth is small compared to the Brillouin frequency shift (hereafter "Brillouin frequency"), which is 16 GHz at 1.06 μm in fused silica, are not necessarily valid. Here we present a scalar broadband model for laser linewidths comparable to, or larger than, the Brillouin frequency, i.e., for acoustic waves where the modulation bandwidth exceeds the carrier frequency. This model reveals the physics of why an important feature of the narrowband model (linear scaling of threshold with seed bandwidth) holds beyond the expected range of validity.

The model also incorporates Fresnel reflections from splices and endcaps. We use the model to calculate the SBS threshold as a function of seed bandwidth for several phase modulation formats, and various endcap reflectivities.

While the acoustic wave equation is second order in time and space, most treatments of SBS reduce it to a first order ordinary differential equation in time, by using the slowly varying amplitude (SVA) approximation and by considering the acoustic wave to be stationary with respect to the optical waves [10]. In our paper, we also consider the acoustic wave to be stationary, but do not use the SVA approximation.

Our paper is an extension of, and a variation on, several previous broadband treatments. In Ref. [11], the SBS threshold is calculated for a passive fiber for several phase modulation formats

#525771 https://doi.org/10.1364/OE.525771
Journal © 2024 Received 8 Apr 2024; revised 26 May 2024; accepted 11 Jun 2024; published 27 Jun 2024

Optics EXPRESS

(sinusoidal, pseudo-random bit sequence (PRBS), Lorentzian white noise, and sinc^2 white noise) at bandwidths up to one third of the Brillouin frequency. In Ref. [12[, the threshold energy is calculated for a passive fiber excited by 30-ns single- and multi-longitudinal mode pulses with spectra that average to a smooth Gaussian, at linewidths up to 1.1× the Brillouin frequency. In Ref. [13] and [14], the analysis is extended to a field with a constant amplitude and periodic modulation where the spectra consist of discrete lines, and the results compared with experiment. The pure sine wave modulation raises the laser linewidth up to 0.75× the Brillouin frequency, and the PRBS modulation rate extends to 0.2× the Brillouin frequency.

Our approach differs from the above in that it treats a high-power amplifier with an active section and a passive delivery fiber, and we transform the second order acoustic wave equations into two first order equations representing waves traveling in opposite directions. When the seed spectral width is comparable to the Brillouin frequency, a backward acoustic wave is generated, which generates an anti-Stokes peak in the backward optical wave. Our approach yields physical insights into why narrow-band models work beyond expectations. For example, our more rigorous approach shows that, in the absence of feedback via Fresnel reflection, the SBS threshold scales linearly with seed bandwidth, at least up to three times the Brillouin frequency.

At the spontaneous level and at room temperature, based on conservation of momentum and energy alone, we could expect to see both Stokes and anti-Stokes photons generated, kT being ~400× larger than the phonon energy. At the stimulated level, a forward-going acoustic wave builds up because forward-going phonons are generated in the Stokes process. A backward-going acoustic wave usually does not build up because such phonons are absorbed in the anti-Stokes process. A backward acoustic wave can however be generated in the case of broadband SBS. This can be seen from an ω,k diagram for the coupling of a forward laser wave (L), a backward Stokes wave (S), and a forward acoustic wave (Fig. 1). The acoustic velocity v_a is exaggerated for clarity, but conservation of momentum and energy are respected in the diagram. The green and red rectangles on the vertical axis illustrate the idealized case of square spectra for the laser and Stokes waves. The laser/Stokes difference frequencies and wavevectors occupy the region shown by the blue oval.

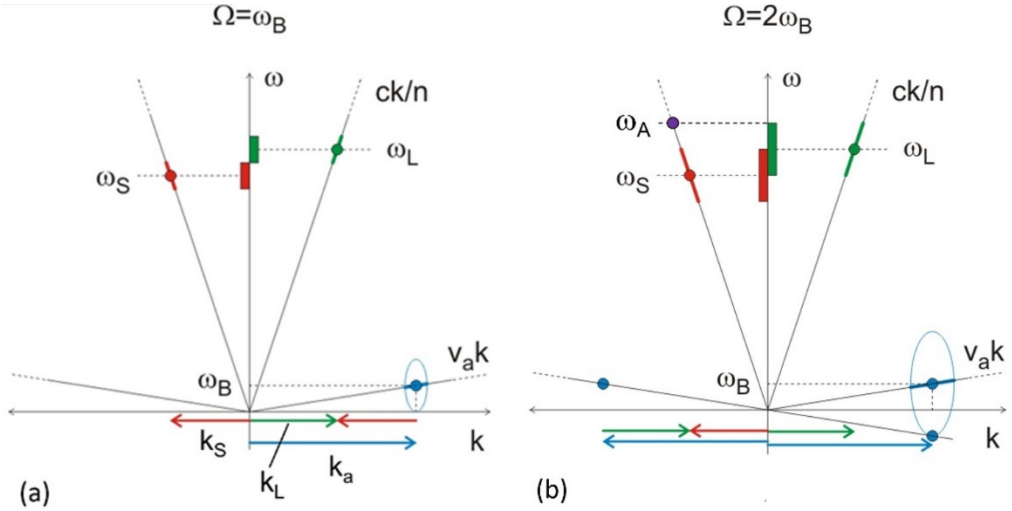

Fig. 1. Frequency-wavenumber (ω,k) diagrams for the optical and acoustic waves in the medium. The acoustic velocity is exaggerated for clarity. The spectrum of the forward optical wave is shown in green, the spectrum of the Stokes wave is shown in red. (a) illustrates the case of a laser spectral width equal to the Brillouin frequency. (b) illustrates the case of a laser spectral width equal to twice the Brillouin frequency, generating an anti-Stokes wave.

Optics EXPRESS

For the case where the laser spectral width, $\Delta\omega_L$ equals the Brillouin frequency, ω_B, the difference frequencies span the range from 0 to $2\omega_B$ (Fig. 1(a)). Through the electrostrictive effect, phonons will build up in the region that is both inside the blue oval and close to the line $\omega = v_a k$, given that the Brillouin linewidth is small compared to the Brillouin frequency.

For the case $\Delta\omega_L = 2\omega_B$, the difference frequencies span the range from $-\omega_B$ to $3\omega_B$, resulting in the generation of a second acoustic wave which propagates in the –k direction (Fig. 1(b)). Scattering from the backward acoustic wave generates a backward-propagating anti-Stokes wave at ω_A (purple dot).

In the broadband case, while the center frequencies still obey the usual relation $\omega_S<\omega_L<\omega_A$, the Stokes wave may have spectral components at frequencies higher than ω_L and the anti-Stokes wave may have spectral components at frequencies lower than ω_L. If the two backward waves cannot be distinguished based on frequency, they must be treated as one wave. Therefore, we adopt the notation E_B instead of the usual E_S. For consistency, we will use E_F instead of E_L in what follows, with the same notation for ρ_B and ρ_F (Fig. 2).

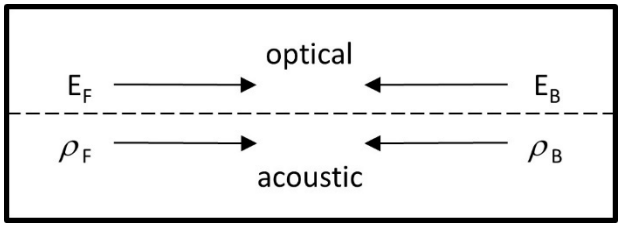

Fig. 2. Geometry of the SBS interaction.

2. Optical wave equation

We begin with the nonlinear wave equation in a homogeneous medium, a good approximation for a well-confined fundamental mode propagating in a step index fiber [10].

$$\nabla^2\tilde{E} - \frac{1}{\epsilon_0 c^2}\frac{\partial^2}{\partial t^2}\tilde{D} = \frac{\gamma_e}{\rho_0 c^2}\frac{\partial^2}{\partial t^2}\tilde{\rho}\tilde{E} \tag{1}$$

$\tilde{\rho}(t,z)$ is the real propagating density field, $\tilde{E}(t,z)$ is the electric field, and $\tilde{D}(t,z)$ is the displacement field. The displacement field, $\tilde{D}$, is given by

$$\tilde{D}(t,z) = \int_0^\infty \varepsilon(\tau)\tilde{E}(t-\tau,z)d\tau. \tag{2}$$

All three fields have components propagating in the forward (F) and backward (B) directions.

$$\tilde{E} = E_F\exp(-i\omega_0 t + ik_0 z) + E_B\exp(-i\omega_0 t - ik_0 z) + c.c. \tag{3}$$

$$\tilde{D} = D_F\exp(-i\omega_0 t + ik_0 z) + D_B\exp(-i\omega_0 t - ik_0 z) + c.c. \tag{4}$$

$$\tilde{\rho} = \rho_F\exp(-i\Omega t + iqz) + \rho_B\exp(-i\Omega t - iqz) + c.c. \tag{5}$$

Here, note that the wavevectors are related by $q = 2k_0$, and $c.c.$ refers to complex conjugate. $\tilde{E}$ and $\tilde{D}$ are separated into sinusoidal parts that vary rapidly in z,t and complex amplitudes that vary relatively slowly. In view of the expectation that the broadband modulation on the optical wave is transferred to the acoustic wave which has a much lower carrier frequency, we make no

Optics EXPRESS

such approximation concerning ρ_F and ρ_B, nor is it necessary, as will be seen later. Following [15], we keep only two terms in the Taylor expansion of $\varepsilon(\omega)$.

$$D_{F,B} = \varepsilon(\omega_0)E_{F,B} + i\varepsilon'(\omega_0)\frac{dE_{F,B}}{dt} \tag{6}$$

Here $\varepsilon'(\omega_0) = (d\varepsilon/d\omega)|_{\omega_0}$, and we assume that ε is the same for E_F and E_B as is ε'. Putting (3)–(6) into (1), we obtain

$$\frac{\partial E_F}{\partial t} + i\,\Omega\,E_S - v_g\frac{\partial E_F}{\partial z} = \frac{i\omega_0\gamma_e}{2n^2\rho_0}[\rho_F\exp(-i\,\Omega t) + \rho_B\exp(i\,\Omega t)]E_B, \text{ and} \tag{7}$$

$$\frac{\partial E_B}{\partial t} + i\,\Omega\,E_S - v_g\frac{\partial E_B}{\partial z} = \frac{i\omega_0\gamma_e}{2n^2\rho_0}[\rho_F^*\exp(i\,\Omega t) + \rho_B^*\exp(-i\,\Omega t)]E_F. \tag{8}$$

3. Acoustic wave equation

The wave equation for the density, $\tilde{\rho}$, has a driving term proportional to the electrostrictive constant γ_e [10]. $\hat{f}_{\text{noise}}$ is the thermal acoustic noise source that initiates Brillouin amplification.

$$\frac{\partial^2\tilde{\rho}}{\partial t^2} - \Gamma'\nabla^2\frac{\partial\tilde{\rho}}{\partial t} - v_a^2\nabla^2\tilde{\rho} = -\frac{1}{2}\epsilon_0\gamma_e\nabla^2\left\langle\tilde{E}^2\right\rangle + \tilde{f}_{\text{noise}}(z,t) \tag{9}$$

The electrostrictive constant is

$$\gamma_e = \rho_0\left.\frac{\partial\varepsilon(\rho_0,S;\omega_0)}{\partial\rho_0}\right|_S \simeq \rho_0\left.\frac{\partial\varepsilon(\rho_0,T;\omega_0)}{\partial\rho_0}\right|_T \tag{10}$$

where ρ_0 is the equilibrium density, S is the entropy, and T is the temperature. The speed of sound is given by $v_a^2 = (\partial p/\partial\rho_0)_s$ where the change in pressure with respect to the equilibrium density is evaluated at constant entropy. The damping coefficient is given by

$$\Gamma' = \frac{1}{\rho_0}\left[\frac{4}{3}\eta_s + \eta_b + \frac{\kappa}{C_p}(\gamma - 1)\right] \tag{11}$$

where the thermodynamic quantities are defined in Ref. 15. $\left\langle\tilde{E}^2\right\rangle$ denotes the time average of $\tilde{E}^2$ over many optical periods.

$$\frac{1}{2}\left\langle\tilde{E}^2\right\rangle = |E_F|^2 + |E_B|^2 + E_F E_B^* e^{iqz} + E_F^* E_B e^{-iqz} \tag{12}$$

For convenience, we write

$$\tilde{f}_n = f_n\,e^{iqz} + c.c. \tag{13}$$

We now insert (5), (12), and (13) into (9), and make the usual approximation that $q^2\rho \gg q\,(\partial\rho/\partial z)$ and $\partial^2\rho/\partial z^2$, making the acoustic wave effectively stationary. Because $v_a \simeq 3\times 10^{-5}(c/n)$, including the propagation would be computationally insignificant.

$$\left(\frac{\partial^2}{\partial t^2} + \Gamma' q^2\frac{\partial}{\partial t} + v_a^2 q^2\right)(\rho_F\,e^{-i\,\Omega t} + \rho_B\,e^{i\,\Omega t}) = \frac{\varepsilon_0\,\gamma_e\,q^2}{2}E_F E_B^*\,e^{-i\,\Omega t} + f_n \tag{14}$$

According to the method of variation of parameters [16], Eq. (14) is completely equivalent to two first order equations, provided $\Omega^2 - (\Gamma/2)^2 \approx \Omega^2$. For typical Brillouin frequencies (10^{10} Hz)

Optics EXPRESS

and linewidths (10^8 Hz), this approximation is good to 3 parts in 10^5. Note that no slowly varying amplitude approximation is needed. Thus, we obtain

$$\left(\frac{\partial}{\partial t}+\frac{\Gamma}{2}\right)\rho_F=\frac{\varepsilon_0\,\gamma_e\,q^2}{2i\,\Omega}E_F E_B^*\,e^{i\,\Omega\,t}+f_F,\ \text{and} \tag{15}$$

$$\left(\frac{\partial}{\partial t}+\frac{\Gamma}{2}\right)\rho_B=\frac{\varepsilon_0\,\gamma_e\,q^2}{2i\,\Omega}E_F E_B^*\,e^{-i\,\Omega\,t}+f_B. \tag{16}$$

Here we have also introduced independent noise sources, $f_F(t,z)$ and $f_B(t,z)$, for the two directions. Although they are correlated because they both stem from f_n, the correlation is of the order $|\Gamma/2\Omega|$, therefore negligible. For the computation, we use a random noise source $\delta-$ correlated in (t,z) with a magnitude given in Ref. 17.

4. Gain in the active fiber

Most previous treatments of SBS at kW levels have considered only passive fiber. The case of practical interest for directed energy is a cladding-pumped active fiber where the laser intensity is strongly z-dependent, and the backward wave experiences laser gain as well as Brillouin gain. We model the gain as a two-level system, e.g., Yb ions, i.e., the population densities are constrained by

$$N_{Yb}=N_1+N_2. \tag{17}$$

The upper-level population density is given by

$$\frac{\partial N_2}{\partial t}=\frac{cn\varepsilon_0}{2}\left(\frac{|E_P|^2\alpha_P}{h\nu_P}+\frac{|E_F|^2\alpha_F}{h\nu_L}\right)-N_2W_{21} \tag{18}$$

where we assume the backward wave intensity is negligible. The level populations together with the cross sections for absorption and emission determine the exponential gain or loss coefficient for the forward and backward waves,

$$\alpha_F=(\sigma_{aL}N_1-\sigma_{eL}N_2)\approx\alpha_B \tag{19}$$

and for the pump wave,

$$\alpha_P=(\sigma_{aP}N_1-\sigma_{eP}N_2). \tag{20}$$

The equation for the propagation of the pump laser is therefore,

$$\left(\frac{\partial}{\partial t}+v_g\frac{\partial}{\partial z}\right)E_P=\frac{-\eta\alpha_P}{2}E_P \tag{21}$$

where η represents the core to cladding area ratio. We add an analogous term representing gain at the laser wavelength to the right-hand side of (7) and (8), with $\eta=1$.

The modified Eqs. (7), (8) and Eqs. (15), (16), (21) are discretized and solved with the forward Euler method on a grid where steps in time and space are related by $n\Delta z=c\Delta t$. Convergence occurs in ~8 transit times. Time averages exclude the first two transits because of transients. The number of grid points along the fiber is chosen to be a multiple, usually four or eight, of the product of transit time and bandwidth, where the bandwidth is taken to be 2Ω plus the seed bandwidth. For purposes of determining the number of grid points, the seed bandwidth is taken to be the bandwidth that contains 85% of the seed power to treat different spectral shapes on similar footing. The initial conditions are the steady-state values of E_F, E_P, N_1, and N_2, with no backward optical wave and no acoustic waves. E_F, E_B, ρ_F, and ρ_B are propagated in time. The pump beam and the inversion retain their original z-dependence throughout the simulation. This is appropriate for exploring the regime at or below threshold in an amplifier where the Brillouin gain and the Yb gain are not so high that the backward wave intensity becomes comparable to that of the forward wave and thus affects the inversion.

Optics EXPRESS

5. Results for a high-power fiber amplifier

The parameters for the simulations that follow are shown in Table 1. The active fiber length is chosen to yield 95% pump absorption at high power. The other fiber specifications correspond to a typical commercial large mode area (LMA) fiber. Simulations run for at least six transit times. Averages exclude the first two transits to avoid the startup transients. The seed power is set at 15 dB below the pump power to avoid numerical instabilities.

Table 1. Parameters used in the simulations.

Fiber core / cladding	25 / 400 µm	v_a	5960 m/s
Active / passive length	6.2 / 2 m	Brillouin linewidth	60 MHz
Pump wavelength λ_P	976 nm	Brillouin frequency	16.24 GHz
absorption cross section at λ_P	2.585×10^{-24} m^2	κ	8.98×10^2
emission cross section at λ_P	2.585×10^{-24} m^2	Λ_e	1.24×10^{-8}
Laser wavelength λ_L	1064 nm	n	1.45
absorption cross section at λ_L	5.128×10^{-27} m^2	γ_e	1.95
emission cross section at λ_L	3.023×10^{-25} m^2		
Yb concentration in core	3.420×10^{25} m^{-3}	Yb upper state lifetime	1 ms

The first series of amplifier simulations has a seed modulated by a random walk in phase yielding a Lorentzian spectrum with a 4-GHz Full-Width-Half-Maximum (FWHM). Figure 3 shows the spectrum of E_B for pump powers of 56 W, 225 W, and 900 W. The corresponding seed powers are 1.77 W, 7.12 W, and 28.5 W. Zero frequency corresponds to the laser center frequency. The amplifier output at threshold is 400 W. We define threshold as occurring when $P_B(0)/P_F(L) = 10^{-5}$, which is a conservative value, comparable to that used in industry. The expected Stokes peak is accompanied by an anti-Stokes peak, even though the seed FWHM is only one-fourth of the Brillouin frequency. The existence of an anti-Stokes peak has not been previously reported.

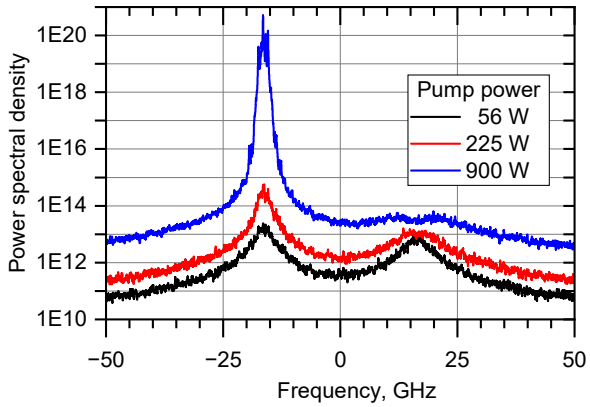

Fig. 3. Spectra of E_B taken at three different pump powers, for a Lorentzian seed spectrum of 4 GHz (FWHM). Zero on the x axis corresponds to the laser center frequency. The Stokes peak is on the left; the anti-Stokes peak is on the right. The output power at threshold is 400 W.

At the lowest power level, the peaks are simply shifted versions of the seed spectrum. The Stokes peak, shown on the left, grows superlinearly with pump power, indicative of the stimulated regime. The anti-Stokes peak grows approximately linearly with pump power, indicative of the

Optics EXPRESS

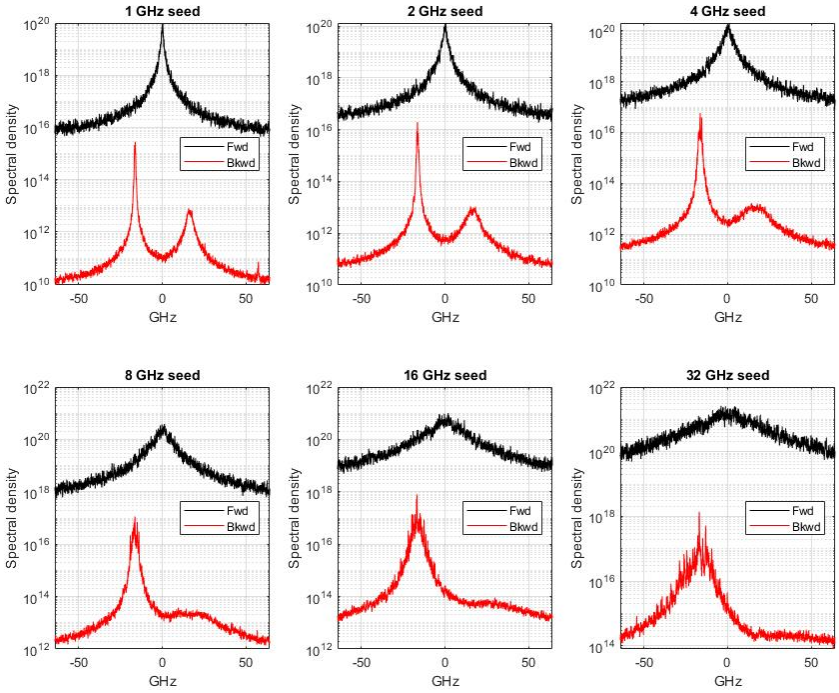

Fig. 4. Spectra of E_F and E_B taken near threshold for a Lorentzian laser bandwidth ranging from 1–32 GHz (FWHM).

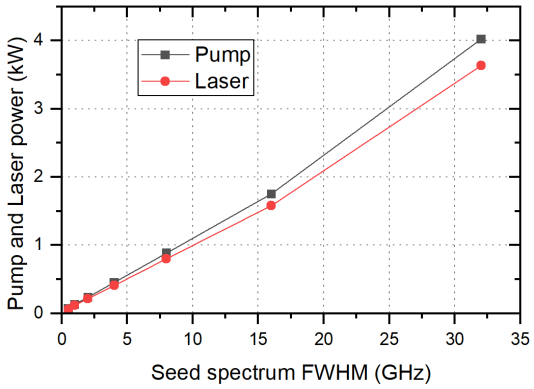

Fig. 5. Pump and laser threshold vs Lorentzian laser bandwidth.

spontaneous regime. Note that the wings of the Stokes (anti-Stokes) peak extend to frequencies above (below) the laser center frequency. A flattening or dip in the middle of the anti-Stokes peak appears near threshold and above. We attribute this to the coupling that causes power flow back to the laser wavelength described by Eqs. (22)–(27) below.

In the next series of simulations, the seed bandwidth and pump power are varied to find the SBS threshold. Figure 4 shows the spectra of E_F and E_B taken near threshold for seed bandwidths ranging from 1-32 GHz (FWHM). The anti-Stokes peak is clearly visible even at a 1-GHz seed bandwidth although it is more than two orders of magnitude lower than the Stokes peak. At a

Optics EXPRESS

bandwidth of twice the Stokes shift, the anti-Stokes peak broadens in proportion to the seed bandwidth and appears as just a shoulder on the Stokes peak.

A plot of threshold pump and laser power vs seed bandwidth shows a linear relationship (Fig. 5) up to a bandwidth of 32 GHz. Therefore, the inclusion of the second derivative in (9), or, equivalently, Eq. (16) for ρ_B, does not change the linear behavior expected from the narrow-band model.

It is apparent from the figures above that the anti-Stokes wave remains orders of magnitude lower in intensity than the conventional Stokes wave.

6. Amplitude of the anti-Stokes wave

There are several factors that govern the amplitude of the anti-Stokes wave. One factor is phase matching, i.e., whether the backward-going phonons generated in Fig. 1(b) have the correct wavevector (and frequency) for coupling the laser and anti-Stokes waves. The Stokes phonons and anti-Stokes phonons differ slightly in frequency and wavevector. The phonon frequency difference is small compared to a 32 GHz laser bandwidth: $\nu_{\text{anti - Stokes}} - \nu_{\text{Stokes}} \simeq 4n\nu_L(\mathrm{v}_a/c)^2 = 0.6\,\text{MHz}$. However, the phonon wavevector difference, $q_{\text{anti - Stokes}} - q_{\text{Stokes}} \simeq 680\,\text{m}^{-1}$, is comparable to the $670\,\text{m}^{-1}$ spread in laser wavevectors associated with a bandwidth of 32 GHz, so phase matching is relevant.

The main reason why the anti-Stokes wave does not grow is that the power flow is from the anti-Stokes wave back to the laser wave. This can be seen from the equations that result from separating E_B into two components, which is valid when they do not significantly overlap in frequency. This separation allows us to compare the growth of both waves in the narrow-band regime. Instead of (3), we divide the total field into Laser, Stokes, and anti-Stokes components.

$$\tilde{E} = E_L\exp(-i\omega_L t + ik_L z) + E_S\exp(-i\omega_S t - ik_S z) + E_A\exp(-i\omega_A t - ik_A z) + c.c. \tag{22}$$

In the narrow-band, steady-state limit, and neglecting the acoustic noise term, we obtain

$$\frac{dE_L}{dz} = +\kappa|E_A|^2E_L \tag{23}$$

and

$$\frac{dE_A}{dz} = +\kappa|E_L|^2E_A - \frac{i\,\Omega}{v_g}E_A \tag{24}$$

in the absence of ρ_F and E_S. The coupling constant is given by

$$\kappa = \frac{\omega_0\gamma_e^2\varepsilon_0 q^2}{2n^2\rho_0\Gamma\Omega\mathrm{v}_g}. \tag{25}$$

Since the waves are counter-propagating, the power flows from E_A to E_L. In the absence of ρ_B and E_A, the power flows from E_L to E_S.

$$\frac{dE_L}{dz} = -\kappa|E_S|^2E_L \tag{26}$$

$$\frac{dE_S}{dz} = -\kappa|E_L|^2E_S + \frac{i\Omega}{v_g}E_S \tag{27}$$

A *forward* anti-Stokes wave does not grow from noise [10, pg. 441] for the same reason. In addition to limiting the amplitude of the anti-Stokes wave, we believe the reverse power flow is responsible for the flattening and dip in the anti-Stokes peak seen in Fig. 3 and Fig. 4.

Optics EXPRESS

7. Influence of a reflection at the fiber end cap

In contrast to the numerical data in Fig. 5, an experimental measurement of SBS in a 1.4 kW amplifier has shown a sublinear dependence of threshold on seed bandwidth [18]. An explanation proposed by the authors was that the modulated laser beam had enough spectral power density 16 GHz below the center frequency that a reflection from the fiber exit face could seed the Stokes wave [19]. Our broadband model easily incorporates Fresnel reflections that occur at splices and at the exit face, and our results described below agree with this hypothesis.

Several papers have analyzed experimentally and theoretically the effect of such a reflection. Evidence of seeding the Stokes wave was seen in a study of PRBS phase modulation in a high-power amplifier which revealed a ~30% decrease in threshold when the modulation frequency was carefully tuned so that a harmonic coincided with the Brillouin frequency [20]. High resolution spectroscopy of the backward wave revealed that it was due to an overlap between a Fresnel-reflected line in the wings of the laser spectrum and one of the peaks in the Stokes spectrum.

The influence of reflections has also been treated theoretically for the case of a passive fiber and pulses with a Gaussian spectrum and FWHM linewidths up to 32 GHz [12-144]. The influence of reflections on SBS in a fiber amplifier seeded by white noise has been studied experimentally at the 500 W level. The rms linewidth was varied from 5-10 GHz [21]. Good agreement was obtained with a steady-state model incorporating a laser wave, backward Stokes wave, Rayleigh scattering, and ASE.

Our work differs from previous work in one or more of the following ways: (a) the model is time-dependent and includes acoustic waves traveling in both directions, (b) the model includes the buildup from distributed noise based on first principles, (c) the model includes a gain and a passive section of the fiber, (d) the model includes a pump beam and inversion in the gain section, and (e) we have analyzed more recent phase modulation formats.

To explore this effect with our model, we introduced a reflection coefficient for E_F at the fiber end face. In addition to the Lorentzian laser spectrum, we investigated a Gaussian spectrum from random phase or frequency modulation, and a flat-top spectrum from triangular frequency modulation [22]. In addition to seeding the Stokes wave, the Fresnel reflection contributes to a peak at the laser frequency and at the anti-Stokes frequency (Fig. 6). The latter two peaks are down by two or more orders of magnitude, so they play only a small role in determining threshold.

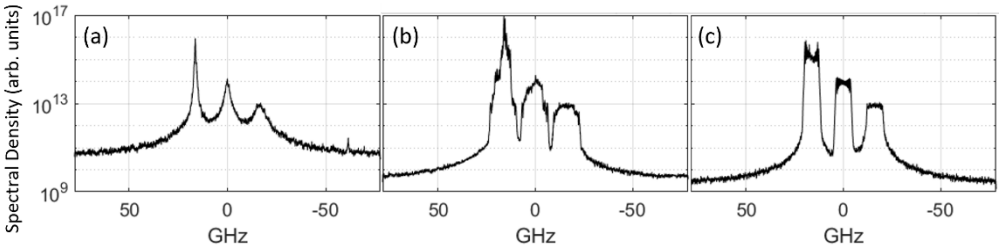

Fig. 6. Spectrum of the backward wave close to threshold for the following conditions: $r = 10^{-4}$ and (a) random walk frequency modulation, (b) random frequency modulation, (c) triangular frequency modulation, all with the same 85% bandwidth of 6.7 GHz. The threshold output powers are 200 W, 394 W, and 568 W.

The various phase modulation formats clearly yield thresholds with different dependence on bandwidth and endcap reflectivity. In the case of a Gaussian spectrum due to random frequency modulation (Fig. 7), the sublinear dependence of threshold on bandwidth is noticeable at $r = 10^{-4}$ but maintains a monotonic rise even at $r = 3 \cdot 10^{-4}$. Figure 7 can be compared to Fig. 2(b) in

Optics EXPRESS

Ref. 18. In the case of a spectrum with sharper edges, e.g., that due to triangular frequency modulation (Fig. 8), the threshold decreases abruptly at 16 GHz where the Stokes and (reflected) laser spectra begin to overlap, seeding the Stokes wave.

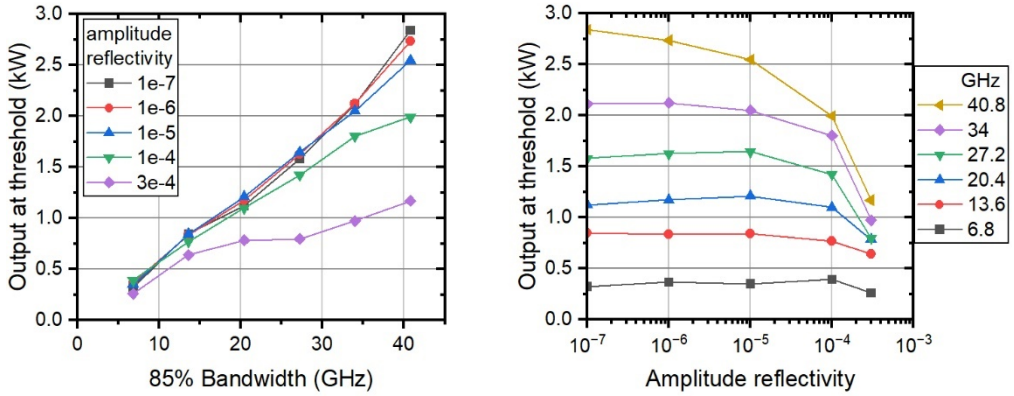

Fig. 7. Results for random frequency modulation. Output power at threshold v (left) bandwidth, and (right) amplitude reflectivity.

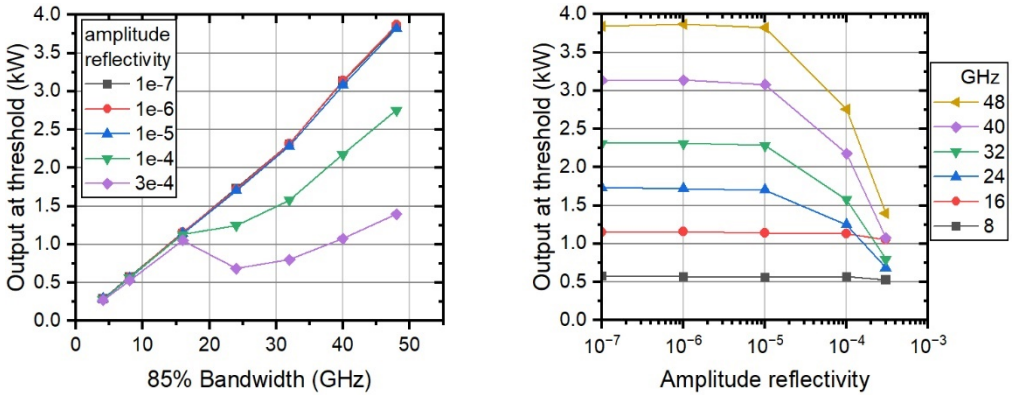

Fig. 8. Results for triangular frequency modulation. Output power at threshold v (left) bandwidth and (right) amplitude reflectivity.

8. Summary

We have presented a model for SBS in a fiber amplifier with a broadband seed. It predicts the existence of a backward propagating acoustic wave accompanied by an anti-Stokes optical wave that has not been previously reported. The anti-Stokes wave remains low in power because its direct interaction with the laser involves power flow in the wrong direction; therefore, its role in the amplifier is limited. The broadband model reveals the physics of why the narrow-band model works well even when the modulation bandwidth is comparable to the Brillouin frequency.

The model is also useful for analyzing cases where Fresnel reflections seed the backward wave. It lends further evidence to support existing hypotheses for the nonlinear dependence of threshold on seed bandwidth. The model indicates to what level the reflections have to be reduced, through anti-reflection coatings and tilted endcaps, to avoid lowering the threshold. And it shows that for non-zero reflectivities, the threshold can decrease with seed bandwidth in certain regimes.

Optics EXPRESS

Funding. High Energy Laser Joint Technology Office (FA9451-15-D-0025/0001); Applied Physics Laboratory, Johns Hopkins University.

Disclosures. The authors declare no conflicts of interest.

A related study has recently presented theoretical and experimental results that show the same general trend as one of the cases presented here, a Gaussian seed spectrum [23]. The authors propose a new spectral evolution model to describe SBS in narrow-linewidth fiber amplifiers in the presence of weak end feedback. An important issue they focus on is how to accurately characterize different end reflections produced by varying the cleave angle.

Data availability. Data underlying the results presented in this paper are not publicly available at this time but may be obtained from the authors upon reasonable request.

References

1. P. Ma, H. Chang, Y. Ma, *et al.*, "7.1 kW coherent beam combining system based on a seven-channel fiber amplifier array," Opt. Laser Techol. **140**, 107016 (2021).
2. F. Tian, H. Yan, L. Chen, *et al.*, "Investigation on the influence of spectral linewidth broadening on the beam quality in spectral beam combination," Proc. SPIE **9255**, 92553N (2015).
3. K. Ludewigt, A. Liem, U. Stuhr, *et al.*, "High-power laser development for laser weapons," Proc. SPIE **1116207**, 2 (2019).
4. J. Ballato, T. Hawkins, M. Cavillon, *et al.*, "The materials science and engineering of optical noninearities and their mitigation in high power lasers," Proc. SPIE **111620G**, 11 (2019).
5. P.D. Dragic, N. Yu, M. Cavillon, *et al.*, "Multicomponent glasses and their application in low nonlinearity optical fiber," Proc. SPIE **PC119810**, 5 (2022).
6. D. Brown, M. Dennis, and W. Torruellas, "Improved phase modulation for SBS mitigation in kW-class fiber amplifiers," *SPIE Photonics West* (2011).
7. B.M. Anderson, R. Hui, A. Flores, *et al.*, "SBS suppression and coherence properties of a flat top optical spectrum in a high power fiber amplifier," Proc. SPIE **10083**, 100830 V (2017).
8. R. Prakash, B.S. Vikram, and V.R. Supradeepa, "Enhancing the efficacy of noise modulation for SBS suppression in high power, narrow linewidth fiber lasers by the incorporation of sinusoidal modulation," IEEE Photonics J. **13**, 1–6 (2021).
9. G.D. Goodno and J.E. Rothenberg, "Suppression of stimulated Brillouin scattering in high power fibers using nonlinear phase demodulation," Opt. Express **27**(9), 13129–13141 (2019).
10. R.W. Boyd, *Nonlinear Optics*, 3rd edition (Academic, 2008).
11. C. Zeringue, I. Dajani, S. Naderi, *et al.*, "A theoretical study of transient stimulated Brillouin scattering in optical fibers seeded with phase-modulated light," Opt. Express **20**(19), 21196–21213 (2012).
12. M.S. Bowers and R.S. Afzal, "Stimulated Brillouin scattering in optical fibers excited by broad-band pump waves in the presence of feedback," Proc. SPIE **87330I**, 87330I (2013).
13. M.S. Bowers, "Stimulated Brillouin scattering in optical fibers with end reflections excited by broad-band, phase-modulated pump waves," Proc. SPIE **9466**, 94660J (2015).
14. M.S. Bowers and N.M. Luzod, "Stimulated Brillouin scattering in optical fibers with end reflections excited by broadband pump waves," Opt. Eng. **58**(10), 1 (2019).
15. L. D. Landau and E. M. Lifshitz, *Electrodynamics of Continuous Media*, 1st edition (Pergamon, 1960), Chap. 61, Eq. (61.8), p. 255.
16. W.E. Boyce and R.C. DePrima, *Elementary Differential Equations and Boundary Value Problems*, 5th edition (Wiley, 1992), Chap. 3, Section 7, pp. 164–168.
17. R. W. Boyd, K. Rzazewski, and P. Narum, "Noise initiation of stimulated Brillouinscattering," Phys. Rev. A **42**(9), 5514–5521 (1990).
18. G.D. Goodno, S.J. McNaught, J.E. Rothenberg, *et al.*, "Active phase and polarization locking of a 1.4 kW fiber amplifier," Opt. Lett. **35**(10), 1542–1544 (2010).
19. G. Goodno and J.E. Rothenberg, private communication.
20. C. Robin, I. Dajani, C. Zeringue, *et al.*, "Pseudo-random binary sequence phase modulation in high power Yb-doped fiber amplifiers," Proc. SPIE **8601**, 86010Z (2013).
21. B.S. Vikram, R. Prakash, V. Balaswamy, *et al.*, "Determination and analysis of line-shape induced enhancement of stimulated Brillouin scattering in noise broadened, narrow linewidth, high power fiber lasers," IEEE Photonics J. **13**(2), 1–12 (2021).
22. J.O. White, J.T. Young, C. Wei, *et al.*, "Seeding fiber amplifiers with piecewise parabolic phase modulation for high SBS thresholds and compact spectra," Opt. Express **27**(3), 2962–2974 (2019).
23. W. Li, Y. Deng, C. Qi, *et al.*, "Evaluation of the impact of weak end feedback on the SBS threshold in high-power narrow-linewidth fiber amplifiers," Opt. Express **32**(9), 16478–16490 (2024).